Catalysis
Science & Technology

RSC Publishing

PAPER

View Article Online
View Journal | View Issue

Cite this: *Catal. Sci. Technol.*, 2013, **3**, 444

Catalytic behavior of MnMCM-48 and WMnMCM-48 ordered mesoporous catalysts in a reductive environment: a study of the conversion of methylcyclopentane

Ioana Fechete,*[a] Ovidiu Ersen,[b] Francois Garin,[a] Liliana Lazar[c] and Alain Rach[a]

Received 4th July 2012,
Accepted 21st September 2012

DOI: 10.1039/c2cy20464a

www.rsc.org/catalysis

Direct hydrothermal synthesis (HT), template ion-exchange (TIE) and molecular dispersion (MD) approaches were used to introduce manganese species into MCM-48-type mesoporous materials. The tungsten was highly dispersed within the channels of mesoporous MnMCM-48 samples by chemical grafting (CG) *via* a liquid–solid reaction. The prepared manganesosilicate and tungstenomanganesosilicate MCM-48-type mesoporous materials were characterized by physico-chemical techniques, including TEM, N_2 sorption, XRD, XPS, UV-Vis and elemental analysis. The physico-chemical characterization revealed that all of the samples retained a high surface area, a regular cubic mesoporosity and that the Mn and W were highly dispersed. The higher unit cell parameter/pore wall thickness values of the MnMCM-48 and WMnMCM-48 samples relative to that of pure MCM-48 indicate the incorporation of Mn and W into the framework/channels of MCM-48. The Mn and W species existed as isolated sites in the framework/extra-framework or as monomolecular species. No bulk manganese or tungsten was observed outside the MCM-48-type mesoporous materials. The coexistence of Mn^{2+}, Mn^{3+} or/and W^{6+} was evidenced by XPS and UV-Vis spectroscopic measurements. The catalytic activities of these samples were studied with respect to the conversion of methylcyclopentane (MCP) in reductive media as a function of Mn loading and reaction temperature (200–500 °C). Whatever the manganese content and irrespective of the temperature of reaction, the MnMCM-48 mesoporous samples did not exhibit catalytic activity, which suggests that the electrophilic manganese oxygen species, operative over all the samples, were inactive sites for the conversion of MCP. The addition of tungsten favored catalytic activity. When the WMnMCM-48 was not calcined, only the methane (C_1) cracking product was observed to be formed by successive rupture of C–C bonds starting at 400 °C. When the WMnMCM-48 was calcined, ring-opening products formed by the C–C rupture, at substituted and unsubstituted carbon atoms, were observed starting at 400 °C. This behavior is associated with a symbiotic process between the MnMCM-48 support and the W nanoparticles.

1. Introduction

Much attention has been directed toward the conversion of methylcyclopentane (MCP) on supported noble-metal catalysts because these catalysts are able to facilitate the reaction with atom economy.[1–4] The conversion of MCP involves the formation of 2-methylpentane (2-MP), 3-methylpentane (3-MP) and *n*-hexane (*n*-H) as desired ring-opening products and the formation of cracking and ring-enlargement products as by-products. The competition among these products is governed by the nature of the metal, the nature of the support and the reaction conditions.[1–10] Two mechanisms for the ring opening of MCP have been observed: the *selective mechanism*, which results primarily in 2-MP and 3-MP, and the *non-selective mechanism*, which forms 2-MP, 3-MP and *n*-H.[11,12] The 2-MP and 3-MP products have been established to form on metal sites, whereas the *n*-H required both metal and acidic sites. Although supported noble-metal catalysts exhibit high activities and selectivities, they suffer from disadvantages that include sensitivity to poisoning, requiring special conditions for their preparation, high price values and limited availability. These limitations are currently driving renewed interest in the

[a] *Laboratoire des Matériaux, Surfaces et Procédés pour la Catalyse, UMR 7515 CNRS, Université de Strasbourg, 25 rue Becquerel, 67087, Strasbourg Cedex 2, France. E-mail: ifechete@unistra.fr; Fax: +33 (0)368852761; Tel: +33 (0)368852737*
[b] *Institut de Physique et Chimie des Matériaux de Strasbourg, UMR 7504 CNRS, 23 rue du Loess BP 43, F-67034, Strasbourg Cedex 2, France*
[c] *Department of Chemical Engineering/Engineering of Inorganic Products, Gh. Asachi University of Iasi, 73 D.Mangeron Bd., 700050, Iasi, Romania*

development of new catalytic systems that do not incorporate noble metals.[13,14]

Non-noble metal oxides constitute an outstanding alternative to the precious metals.[13] Non-noble metal oxides are used in many catalytic applications, including hydrodesulfurization,[15] methanol decomposition to hydrogen, methane and CO,[16] the N_2O oxidation of benzene to phenol,[17,18] the reduction of environmental pollution olefin epoxidation,[19] the conversion of aromatic hydrocarbons[20,21] and Aldol/Prins condensations[22,23] because they are less costly. Among the non-noble metal oxides, the manganese oxides, in particular, have been a key topic of investigation because of their potential catalytic applications[24–30] which can be conducted in oxidative environments.

Until now, no studies on the conversion of MCP on manganese oxides under a reductive environment have been reported. However, recent research in the area of catalysis for MCP conversion has concentrated on the development of alternative catalysts, especially supported tungsten, iron and molybdenum catalysts.[14,31,32] These catalysts have demonstrated that the catalytic activity of the catalyst is dependent on the density of active sites, the dispersion, and the location and coordination of the metal atoms.[14,31,32] The role of the support is dominant, which indicates that it must have a high surface area to disperse a large fraction of the active metal phase. By dispersing the metal in this way, a large total area of metal surface is available for catalytic reactions to occur. A high metal particle dispersion is desirable to achieve a high level of catalytic conversions.[14,31,32]

The discovery of the MCM-48 siliceous mesostructured material has attracted considerable attention as a catalyst support because this material possesses a high surface area and an ordered cubic structure with a controllable, uniform pore size.[33] MCM-48, because of its cubic structure, has been suggested to be a more advantageous system than MCM-41 for catalytic applications because the three-dimensional pore system of MCM-48 may allow faster diffusion through the channels and make this material more resistant to pore blocking.[14,34]

Nonetheless, no previous studies on MCM-48-supported manganese oxides in a reductive environment have been reported. This knowledge gap provides an opportunity to enrich our understanding of manganese oxides for the conversion of MCP with hydrogen at atmospheric pressure. The purpose of this work is to investigate the oxidation state and the local environment of manganese species, their spatial distribution (framework/inside the pores), and their role in the conversion of MCP. The reactivity of MnMCM-48 catalysts prepared using different strategies, such as hydrothermal synthesis, ion template exchange, and designed metal dispersion, were evaluated for the first time in the conversion of MCP in the temperature range of 200 to 500 °C. The tungsten was dispersed by chemical grafting *via* a liquid–solid reaction.

2. Experimental part

2.1. Materials and instrumentation

Cetyltrimethylammonium bromide (CTAB), manganese acetylacetonate $Mn(acac)_3$ and tungsten hexachloride (WCl_6) (99%) were purchased from Sigma-Aldrich. Manganese acetate tetrahydrate $(CH_3COO)_2Mn{\cdot}4H_2O$, potassium permanganate ($KMnO_4$) and sodium hydroxide (NaOH) 98% were purchased from SDS. Tetraethylorthosilicate (TEOS) 98% was purchased from Acros. The methylcyclopentane (MCP) used for the catalytic tests was supplied by Aldrich (puriss >99%). All chemicals were used as received.

Transmission electron microscopy (TEM) images were obtained on a TopCon 2100 FCs microscope operated at an accelerating voltage of 200 kV. The samples were dispersed in ethanol in an ultrasonic bath for several minutes and then deposited on a Cu grid and dried at room temperature. *Nitrogen sorption* measurements were performed at −196 °C on a TriStar instrument. The samples were first outgassed at 250 °C overnight. The linear part of the Brunauer–Emmett–Teller (BET) equation[35] was used to determine the specific surface area. The pore size distribution curves were calculated from the desorption branches of the isotherms using the Barett–Joyner–Halenda (BJH) method.[36] The mean thickness of the pore wall (w) of the cubic structure in the MCM-48 mesoporous solid was calculated according to the formula $w = (a_0/3.092) - (D_{BJH}/2)$, where a_0 is the unit cell parameter, 3.092 is a constant that represents the minimal surface area for the MCM-48 space group,[37] and D_{BJH} is the pore diameter. The cumulative pore volume (V_{BJH}) of the mesopores was obtained from the amount of nitrogen adsorbed at a relative pressure p/p_0 of 0.99,[38] assuming complete surface saturation with nitrogen. *Powder X-ray diffraction* (XRD) patterns were recorded on a Bruker D8 powder diffractometer equipped with a CuKα radiation source (λ = 0.154 nm) operated at 40 kV and 100 mA. The diffractograms were recorded in the 2θ range of 0.5–5° (low angle) and 10–90° (wide angle). The scans were performed with a step size of 0.02° and a step time of 1.2 s. The unit-cell parameter (a_0), $a_0 = d\{hkl\}\,(h^2 + k^2 + l^2)^{1/2}$ for the $Ia3d$ symmetry group, was evaluated using the interplanar spacing (d) of the (211) XRD peak. *X-ray photoelectron spectroscopy* (XPS) spectra were recorded on a Multilab 2000 spectrometer equipped with an AlKα X-ray radiation source (1486.6 eV) operated at an anode current of 20 mA and 10 keV. The XPS measurements were performed in a static *in situ* reaction chamber at room temperature and at a base pressure of 10^{-9} Pa. The samples were outgassed in a vacuum oven overnight before the XPS measurements. The binding energies of the Mn and W photoelectron peaks were corrected for charge effects based on the C 1s peak at 284.6 eV as reference in the XPS measurements. Peak decomposition was performed using curves that were 85% Gaussian type and a 15% Lorentzian type and using a Shirley non-linear sigmoid-type baseline. The following peaks were used for the quantitative analysis: C 1s, W 4f, and Mn 2p. Based on the XPS analysis, the XPS surface ratio of Si/Mn or/and Si/W is defined as the molar concentration of the Si element (%) divided by the molar concentration of Mn or W (%). The atomic concentrations of all elements were estimated based on comparisons of the integrated peak intensities normalized by the atomic sensitivity factors.[39,40] BEs were reproducible to within ±0.2 eV. *UV-Vis reflectance absorption* spectra were recorded on a PerkinElmer spectrophotometer under computer guidance. Spectra were recorded between 200 and 800 nm and are presented as normalized spectra. The *chemical analysis* of the solid samples was performed at the Service Central d'Analyse of CNRS-Solaize, France.

In this article we have presented the physico-chemical characterization of the calcined samples. It must be noted that the physico-chemical characterization of the reduced catalysts has been performed but no changes were observed and that only the calcined samples, which are stable under reductive conditions up to 500 °C, have been presented here.

2.2. Catalysts preparation

Manganese was introduced onto the MCM-48 support by hydrothermal synthesis (HT), template ion exchange (TIE) and molecular dispersion (MD) approaches. The tungsten was dispersed on MnMCM-48 (HT) Si/Mn = 45 sample following chemical grafting (CG) by a liquid–solid reaction.

2.2.1. MnMCM-48 preparation using direct hydrothermal (HT) synthesis. MnMCM-48 mesoporous solids with Si/Mn molar ratios of 75 and 45 were synthesized hydrothermally under basic conditions following the procedure described elsewhere[14] with manganese acetate substituted for sodium tungstate. The molar gel composition was 1.0 TEOS : (0.02–0.1) Mn : 0.48 CTAB : 0.25 Na_2O : 55 H_2O. In a typical synthesis, the cetyltrimethylammonium bromide, doubly distilled water and sodium hydroxide were stirred for 0.5 h at room temperature, and the tetraethylorthosilicate was added with vigorous stirring.[14] After 0.5 h, the required amount of manganese acetate was added. The gel mixtures were stirred for 3 h at room temperature. The prepared gel mixture was transferred to an autoclave and aged for 72 h at 110 °C. The white precipitate was filtered, washed with distilled water and dried for 24 h at 60 °C. The surfactant was removed using an extraction procedure,[14] and the sample was calcined at 500 °C for 5 h in a muffle furnace with a heating rate of 1 °C min^{-1}. The catalysts were denoted MnMCM-48 (HT).

2.2.2. MnMCM-48 preparation using a template ion-exchange (TIE) procedure. Two samples of MnMCM-48 with Si/Mn molar ratios of 75 and 45 were prepared using a TIE procedure. This procedure was a slightly modified version of that reported by Suib's group.[41] In particular, the as-synthesized MCM-48 support was immersed in 300 mL of $KMnO_4$ aqueous solution that contained the calculated amount of manganese. The obtained suspension was stirred for 10 h at room temperature. The samples were subsequently filtered, washed and dried at 80 °C. The solids were calcined at 500 °C for an isothermal period of 8 h in a muffle furnace with the heating rate of 1 °C min^{-1}. The catalysts were denoted MnMCM-48 (TIE).

2.2.3. MnMCM-48 preparation using a molecular dispersion (MD) process. Two samples of MnMCM-48 with Si/Mn molar ratios of 75 and 45 were prepared using a molecular designed dispersion process. The procedure was adapted from the work reported by Vansant *et al.* for VO_x.[42] The calcined MCM-48 support was introduced into 200 mL of toluene that contained the necessary amount of manganese, and the mixture was stirred for 8 h at room temperature. The samples were filtered, washed and dried at 40 °C. The solids were calcined at 500 °C for 8 h in a muffle furnace heated at 1 °C min^{-1}. The catalysts were denoted MnMCM-48 (MD).

2.2.4. Synthesis of the Si-MCM-48 support. The pure Si-MCM-48 support was synthesized using the same procedure used for the Mn-MCM-48 by a direct hydrothermal method.[14]

2.2.5. Synthesis of the WMn-MCM-48 via chemical grafting (CG) using a solid–liquid reaction. The sample of MnMCM-48 (HT) with a Si/Mn ratio of 45 was immersed in a mixed solution of toluene/ethanol that contained an amount of tungsten necessary to achieve a Si/W molar ratio of 45. The mixture was refluxed under an inert atmosphere for 2 h; this mixture was subsequently introduced into a Teflon autoclave and heated at 100 °C for 8 h. After the autoclave procedure, the product was filtered, washed, dried at 100 °C and calcined at 500 °C for 6 h. The catalysts were denoted WMnMCM-48 (CG).

2.3. Catalytic tests

Reaction of MCP was carried out using a pulse method with hydrogen under atmospheric pressure. The mass of catalysts used was 200 mg and the injected volume of methylcyclopentane was 5 μl. The gas flow used for treatments and catalytic tests was fixed at 40 cm^3 min^{-1}. The catalytic products were analyzed by gas chromatography using a 50 m (CP-SIL-5CP) column and a flame ionization detector (FID). The catalytic activity and performance of the catalysts were measured in terms of conversion and selectivity which are defined as follows:

$$\text{Conversion, } C = \frac{\sum_{i=1}^{n}(i/n)C_i}{C_n^0 + \sum_{i=1}^{n}(i/n)C_i} \times 100 \quad (\text{mol}\%)$$

$$\text{Selectivity, } S_i = \frac{C_i}{\sum_{i=1}^{n} C_i} \times 100 \quad (\text{mol}\%)$$

where C_i is the mole percent of product with i carbon atoms and C_n^0 is the mole percent in the feed of MCP (n = 6).

3. Results and discussion

3.1. Catalyst preparation and elemental analysis

The incorporation of manganese at different Si/Mn ratios into the MCM-48 mesoporous matrix was performed using three approaches:

3.1.1. Direct hydrothermal synthesis. The manganesosilicate solids were formed in basic media using an electrostatic pathway where the head groups of the cationic CTMAB surfactant attract negatively charged inorganic precursors to the surface of the supramolecular assemblies prior to condensation of the inorganic species. Various authors have reported the incorporation of manganese entities into MCM-48 using this procedure.[28,43,44] As shown in Table 1, the Si/Mn ratio in the calcined samples is approximately the same as the Si/Mn ratio in the mixture gel, which indicates an efficient incorporation of the Mn into the framework of MCM-48 *via* the S^+I^- mechanism in basic media. This result is similar to those previously observed and reported in the excellent review of Tusar *et al.*[44]

3.1.2. The template ion-exchange procedure. This procedure is a post-synthesis approach in which the siliceous as-synthesized solid MCM-48 was used as a matrix for manganese species. In this case, the incorporation of manganese ions is expected to

Table 1 Physico-chemical characterization of MnMCM-48 and WMnMCM-48 mesoporous catalysts

Catalyst	Si/Me[a]	Si/Me ICP	Si/Me XPS	Unit cell parameter, a_0 (nm)	Unit cell volume, V (nm^3)	Surface area, BET ($m^2\ g^{-1}$)	Pore volume, V_p ($cm^3\ g^{-1}$)	Pore diameter, D_p (nm)	Pore wall thickness, w (nm)
SiMCM-48	—	—	—	7.86	485.60	1265	1.21	2.34	1.37
MnMCM-48 (HT)	75	82	89	7.92	496.80	1250	1.20	2.34	1.39
MnMCM-48 (HT)	45	54	61	8.01	513.92	1208	1.18	2.34	1.42
WMnMCM-48 (CG)	45	57 W 49 Mn	64 W 54 Mn	8.12	535.38	1130	1.03	2.36	1.44
MnMCM-48 (IE)	75	81	87	7.98	508.16	1252	1.18	2.34	1.41
MnMCM-48 (IE)	45	49	57	8.07	525.55	1190	1.14	2.36	1.42
MnMCM-48 (DM)	75	86	91	7.88	489.30	1230	1.18	2.34	1.38
MnMCM-48 (DM)	45	54	57	7.97	506.26	1181	1.07	2.30	1.42

[a] Me: metal (Mn, W), HT: hydrothermal, CG: chemical grafting, TIE: template ion exchange, MD: molecular dispersion.

occur *via* an anion-exchange approach[41,44] between the uncondensed double 4-ring (D4R) silicate anions and MnO_4^-. Thus, the MnO_4^- ions locate between S^+ and the silica walls, thereby compensating the electronic interactions in the structure. The Si/Mn ratios measured by ICP show that a significant amount of the manganese was incorporated into the mesoporous matrix (Table 1).

3.1.3. Molecular dispersion approach. In this approach the siliceous MCM-48 calcined solid was used as a host for manganese species introduced by $Mn(acac)_3$, which was used as a manganese precursor. The Mn was anchored to the mesoporous surface by hydrogen bonding between the acetylacetonate ligand and the surface hydroxyl groups of the MCM-48 mesoporous support. The Si/Mn ratios measured by ICP show that a significant amount of the manganese was deposited into the mesoporous matrix. The results are presented in Table 1 and indicate that the loss of Mn during the calcination procedure was very low. Similar results have been communicated by Tusar *et al.*[44]

3.1.4. Chemical grafting. The tungsten was added to MnMCM-48 (HT), Si/Mn ratio of 45, *via chemical grafting* using a solid–liquid reaction. The grafting was accomplished by reacting WCl_6 with the surface hydroxyl groups of MnMCM-48 *via* a solid–liquid reaction through chemical bonds. The Si/W ratio was determined by ICP and indicates that the tungsten was grafted onto the MnMCM-48 surface (Table 1).

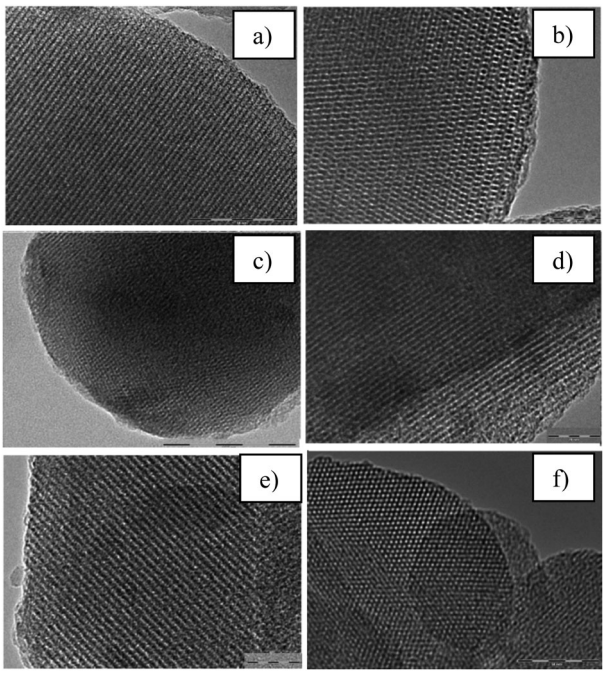

Fig. 1 TEM images of calcined SiMCM-48 (a), MnMCM-48 with Si/Mn = 45 prepared by HT (b), TIE (c), MD (d) approaches and WMnMCM-48 (CG) (e and f) samples.

3.2 Structural characterization

We performed TEM experiments to obtain information about changes in the mesoporous structure and in the Mn and W species during their incorporation into the MCM-48 mesoporous matrix. Fig. 1 shows TEM images of the purely siliceous MCM-48, the manganese and tungsten manganese MCM-48 calcined samples. The ordered arrangement of lattice dots along the [100] direction indicates that the samples have excellent textural uniformity. These results also indicate that the ordered mesoporous structure of the support was unambiguously unaffected by the manganese and tungsten species; the cubic arrangement is maintained for all the samples, and no large aggregates were observed outside of the mesopores. In this case, the MCM-48 is a good matrix for highly dispersed Mn and W species. Similar observations have been reported in the literature for the Mn-MCM-48, Cr-MCM-48, V-MCM-48 and W-MCM-48.[14,28,41]

The maintenance of the ordered cubic arrangement of the MCM-48 frameworks upon the introduction of manganese is further supported by the N_2 sorption data. N_2 sorption isotherms for all the samples are illustrated in Fig. 2. As shown in this figure, at a relative pressure of $p/p_0 \leq 0.3$, the nitrogen adsorption occurs as a monolayer. The isotherms exhibited sharp inflections characteristic of capillary condensation within mesopores, which occurred at p/p_0 = 0.2–0.3. The sharpness of this step indicated a uniform size pore system of the high quality of the MCM-48 samples. These results suggest also that the pore channels are not obstructed. The textural properties of these mesoporous materials are listed in Table 1, which details the BET specific surface area (S_{BET}), the pore volume (V_p), the mesopore diameter (D_{BJH}), which were calculated from the desorption branch of the nitrogen sorption isotherms. Although the incorporation of Mn led to a decrease in the BET specific

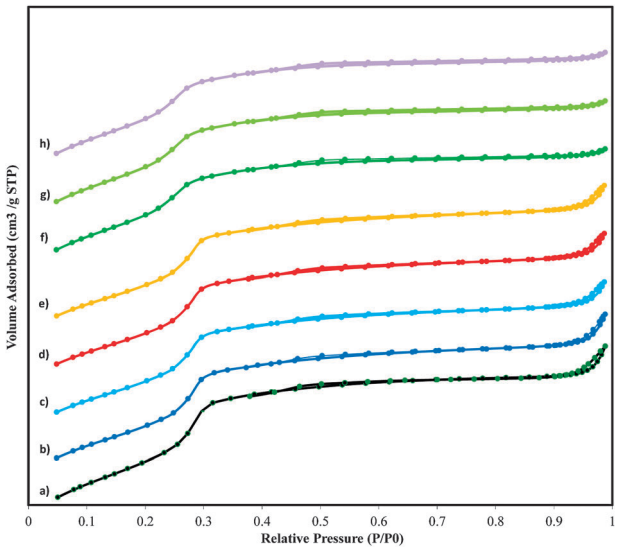

Fig. 2 Nitrogen sorption isotherms at −196 °C for SiMCM-48 (a), MnMCM-48 prepared by HD with Si/Mn = 75 (b), Si/Mn = 45 (c), TIE with Si/Mn = 75 (d), Si/Mn = 45 (e), MD with Si/Mn = 75 (f), Si/Mn = 45 (g) and WMnMCM-48 (CG) (h) samples.

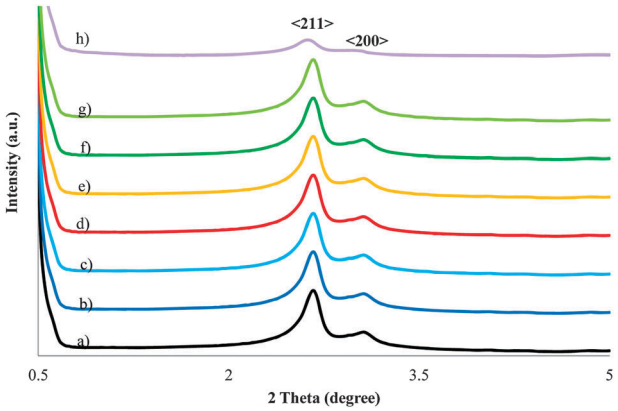

Fig. 3 X-ray diffraction pattern for the calcined SiMCM-48 (a), MnMCM-48 prepared by HD with Si/Mn = 75 (b), Si/Mn = 50 (c), TIE with Si/Mn = 75 (d), Si/Mn = 50 (e), MD with Si/Mn = 75 (f), Si/Mn = 50 (g) and WMnMCM-48 (h) samples.

surface area, high surface areas are observed in MCM-48 with Mn loadings up to a Si/Mn ratio of 45. Similar effects on the BET specific surface area and pore volume have been previously reported.[14,41] A high BET specific surface area was observed even for the WMnMCM-48 sample. We therefore concluded that well-organized mesoporous MCM-48 catalysts with a high surface area could be obtained using all of the described procedures. The total pore volume decreased from the pure silica MCM-48 to the MnMCM-48 with a Si/Mn ratio of 45 and finally to the WMnMCM-48 with Si/W and Si/Mn ratios of 45. The value of mesopore diameter (D_{BJH}) does not change drastically from one approach to another. In all samples pore blockage does not appear, and the manganese species are most likely located in the framework (HT approach) or on the inner surface of the pore channels (TIE and DM approaches). The values of the wall thickness are summarized in Table 1. The wall thickness of the MnMCM-48 and WMnMCM-48 samples increased with increasing manganese/tungsten content, and the walls were denser than those of pure silica MCM-48. These results are consistent with the results reported in the literature.[14]

Fig. 3 shows the powder X-ray diffraction patterns for calcined samples of the pure silica MCM-48, the MnMCM-48 and of the WMnMCM-48 mesoporous materials with different metal contents in the low-angle range from $0.5^\circ < 2\theta < 5^\circ$. The XRD patterns exhibit exclusively (211) and (200) planes belonging to the *Ia3d* cubic symmetry reported for the MCM-48 mesostructure and imply a high degree of order in the mesoporous materials.[33] No remarkable shifts in the diffraction peaks to higher or lower 2-theta values were observed with increasing Mn content.

Moreover, the intensity of the d_{211} peak is gradually attenuated with increasing Mn content in the XRD patterns of the samples. An important decrease in intensity was observed for the WMnMCM-48 sample prepared by chemical grafting. However, the addition of W to MnMCM-48 (HT) of Si/Mn = 45 sample does not significantly alter the degree of order in the mesoporous materials. Logically, the reduced intensity of the reflections may be caused by a degradation of the cubic arrangement of the MCM-48 pores. As evident from the TEM and N_2 adsorption data, the cubic arrangement of the MCM-48 framework was retained after Mn and W were incorporated. In this case, the progressive reduced intensity of the d_{211} reflections is likely due to a dilution of Si with the continuous incorporation of Mn (W) as a consequence of the greater X-ray absorption factor of Mn (W) relative to that of Si. The absorption of X-rays by Mn (W) was indeed significant, as indicated by the strong reduction of the main beam intensity. These results are consistent with those previously reported.[14,28,41,44,45] The cubic *Ia3d* unit-cell parameter (a_0) was calculated using Bragg's equation from d_{211}, which was obtained from the (211) peak in the XRD pattern. The values of the unit-cell parameter from the manganese samples increase with increasing manganese/tungsten content for all the samples. This behavior is similar to those observed for the unit cell volume, *V*. These results are in line with those already reported[44] and indicate the incorporation of Mn atoms into the framework and on the inner walls of the MCM-48 matrix. The change in the unit-cell parameter for the Mn and MnW samples can also be rationalized, in terms of bond lengths. The W–O and Mn–O bonds are longer than the Si–O bond, and the crystal radii of W and Mn are larger than that of Si. These results are consistent with results reported in the literature.[14,41,44]

The high-angle X-ray diffraction patterns ($10^\circ < 2\theta < 90^\circ$) for the MnMCM-48 and WMnMCM-48 samples with various loadings are shown in Fig. 4. The XRD patterns in the high-angle area for all the samples show no distinct reflection of Mn/W oxide phases. This result suggests the presence of very small, well-dispersed species within the silica matrix or on the silica walls. Only a broad maximum centered at $2\theta = 23^\circ$ was observed, which was attributed to amorphous silica; the presence of this maximum suggests a low overall degree of crystallization of siliceous walls. As evidenced by the TEM, BET and XRD results, the ordered mesoporous structures of all the samples were maintained after the Mn and W were incorporated into the MCM-48 structures.

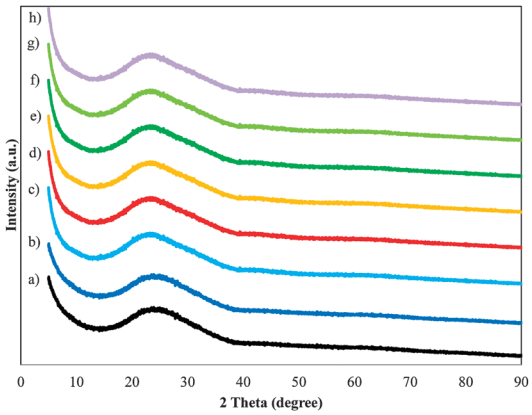

Fig. 4 X-ray diffraction pattern for the calcined SiMCM-48 (a), MnMCM-48 prepared by HD with Si/Mn = 75 (b), Si/Mn = 45 (c), TIE with Si/Mn = 75 (d), Si/Mn = 45 (e), MD with Si/Mn = 75 (f), Si/Mn = 45 (g) and WMnMCM-48 (h) samples.

3.3. Spectroscopic characterization

The valence bond of Mn and the oxidation states of the catalyst surface entities were examined by XPS analysis. The Mn 2p XPS spectra for the calcined Mn catalysts prepared by various approaches are shown in Fig. 5. The energy position and the shape of the two photoelectron peaks are approximately the same for all the samples. For the samples with a Si/Mn ratio of 45, the binding energy values were 641.5 eV and 652.9 eV with a spin–orbit splitting of 11.4 eV. These binding-energy values for Mn are consistent with those of manganese oxide and are in agreement with other results reported previously.[41,46] A comparison of the spectra of samples with a Si/Mn ratio of 75 with those of samples with a Si/Mn ratio of 45 reveals that the spectral shape remains unchanged; however, the change in peak intensities was observed and is more intense for samples with high concentrations of Mn. However, the assignment of the oxidation state of

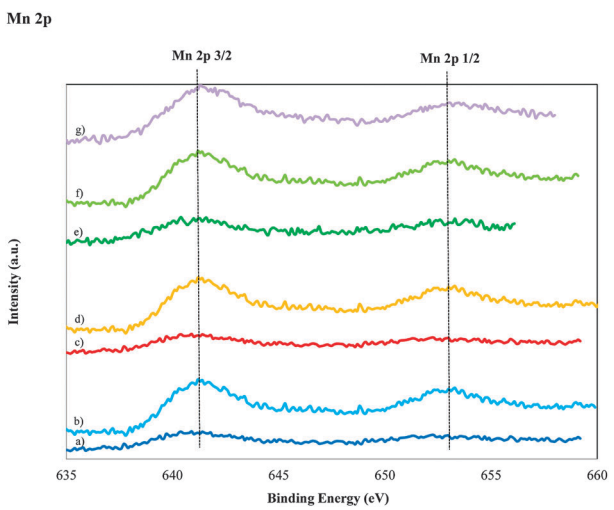

Fig. 5 XPS spectra of the Mn 2p XPS region for calcined MnMCM-48 and WMnMCM-48 catalysts; MnMCM-48 prepared by HD with Si/Mn = 75 (a), Si/Mn = 45 (b), TIE with Si/Mn = 75 (c), Si/Mn = 45 (d), MD with Si/Mn = 75 (e), Si/Mn = 45 (f) and WMnMCM-48 (g) samples.

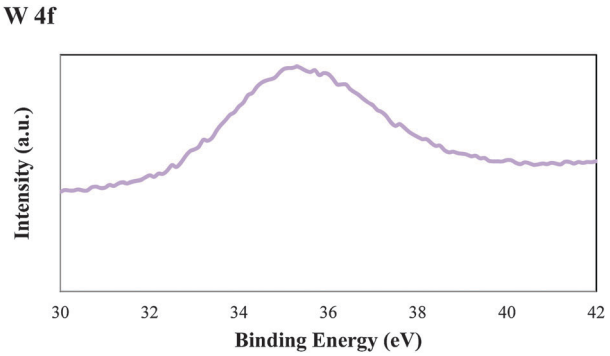

Fig. 6 XPS spectra of the W 4f region for the calcined WMnMCM-48 catalyst.

manganese oxide is difficult because these binding-energy values correspond to several oxidation states, including Mn^{2+}, Mn^{3+} and Mn^{4+}, which funds the assertion that several oxidation states are present on the surface of MnMCM-48 catalysts, irrespective of the manganese concentration and the preparation approach. According to literature data, the binding-energy values of 640 eV, 641 eV, and 641.7 eV correspond to Mn^{2+}, values of 641–642 eV and 641.60 eV correspond to Mn^{3+}, and 642 eV and 642.65 eV correspond to Mn^{4+}.[41,47–49] Based on this analysis, the XPS peak binding energies alone are not sufficient to accurately determine the chemical state of Mn in the manganese oxides.

Fig. 6 shows the W4f peak of the WMnMCM-48 catalyst. The major peak W4f7/2 appears at 35.5 eV and assigned to W^{6+}. This binding-energy value for W is consistent with those of tungsten oxide reported in the literature.[50]

The calculated Si/Mn and Si/W ratios from integral intensities of Si 2p, Mn 2p and W 4f photoelectron spectra are summarized in Table 1. A slight but systematic increase in the Si/Mn and Si/W ratios was observed compared with the chemical analysis.

The identification and characterization of the coordination environment of Mn and W and their locations in the framework/extraframework positions of MCM-48 samples were performed by diffuse-reflectance UV–Vis spectroscopy. Fig. 7 shows the diffuse-reflectance UV–Vis spectra of calcined MnMCM-48 samples with different Mn contents prepared by three methods and also that of the WMnMCM-48 (CG) sample.

The spectra were acquired over the entire ultraviolet and visible regions (200 to 800 nm). The samples with a Si/Mn ratio of 75, prepared by the HT and TIE methods, showed only one absorption band maximum at 270 nm, while the sample with the same Si/Mn ratio prepared by the MD exhibited two overlapped absorption bands at 270 and 500 nm. The absorption maxima are quasi-identical with those reported in the literature.[51,52] When the Mn content was increased (Si/Mn = 45), the peak position of the band shifted to 280 nm, and the absorption edge also shifted to a longer-wavelength position. The less resolved and broad absorption band at a wavelength less than 270 nm is attributed to a ligand-to-metal charge transfer of O^{2-} to Mn^{3+} in a tetrahedral coordination that involves, in this case, isolated transition-metal sites. The Mn^{3+} ions are probably coordinated with the Si and located in the framework

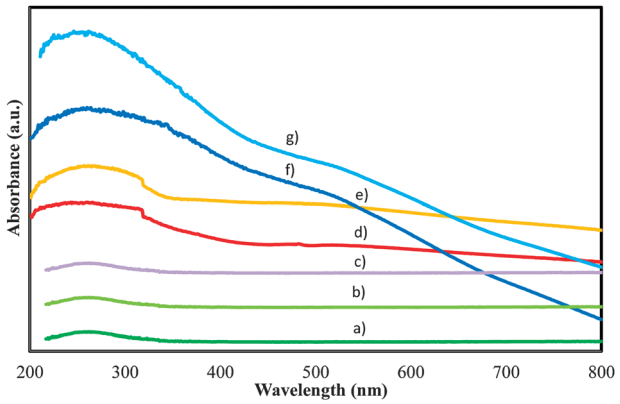

Fig. 7 Diffuse reflectance UV-Vis spectra for the calcined WMnMCM-48 CG (a), MnMCM-48 prepared by HT with Si/Mn = 75 (b), Si/Mn = 45 (c), TIE with Si/Mn = 75 (d), Si/Mn = 45 (e), MD with Si/Mn = 75 (f), Si/Mn = 45 (g) samples.

of MCM-48. These structural features are not rare because they have been observed by other authors.[51–53] The broad absorbance at approximately 500 nm, which was observed in the spectra of the samples prepared by MD, is associated with the d–d transition in Mn^{2+}/Mn^{3+}, which suggests that the two sites should coexist in these samples. Similar results have been reported for the other structures.[51,52,54] Moreover, this band was attributed to the $^6A_{1g} \rightarrow {}^4T_{2g}$ crystal-field transition.[52,54] Our results confirmed that both Mn^{3+} and Mn^{2+} sites are present in the MnMCM-48 (MD) and also support the XPS analysis that multiple Mn oxidation states are present in these samples.

3.4. Catalytic reactivity toward the conversion of MCP

Oxide catalysts have recently been considered a modern alternative to noble-metal catalysts and represent a scientific, economic and ecological challenge.[13] In this work, the well-organized cubic MnMCM-48 and WMnMCM-48 mesoporous solids were investigated as a novel catalyst system for the conversion of MCP. Previously reported results have shown that MnMCM-48 mesoporous catalysts deliver excellent results in oxidative media,[24–30] and we applied the same catalysts in reductive media. The chemistry of these catalysts in reductive media was unknown, and, to our knowledge, these results represent the first catalytic tests of MCP on MnMCM-48 and WMnMCM-48 mesoporous oxides. The catalysts with variable Mn contents and with the same W loadings were evaluated as a function of the reaction temperature in the range of 200 to 500 °C. As observed with noble-metal catalysts tested under the same conditions,[3,6,9] the possible products formed in the conversion of MCP are 2-methylpentane, 3-methylpentane and *n*-hexane, which are formed from a *ring-opening* reaction of MCP. Cyclohexane and benzene can be formed *via ring-enlargement* reactions, whereas methane, ethane, propane, butane, *i*-butane and pentane/*i*-pentane can be formed from *cracking* reactions.

3.4.1. MnMCM-48 catalysts. Irrespective of the method of preparation and the manganese content in the mesoporous manganesosilicate MCM-48 catalysts, no catalytic activity was observed in the temperature range of 200 to 500 °C. Moreover, the reduction treatment under hydrogen of all the catalysts for 30 min, 4 h, 12 h, 24 h or 48 h between 300 and 500 °C did not favor catalytic activity. Although the lingering issue, under the conditions used here, is the relationship between the structure of a catalyst surface and the catalytic activity exhibited by that surface, these features are expected given the physico-chemical characterization results of the Mn catalysts, which show a high specific surface area with Mn sites present on the catalyst surface. The Mn sites consist of highly dispersed species in tetrahedral/octahedral coordination and coexist as Mn^{2+} and Mn^{3+} in the framework and on the inner surface of the mesoporous silicomanganese catalysts, irrespective of the preparation strategies. We tentatively attributed this behavior to the low capacity of manganese sites to dissociate the C–H bonds under our experimental conditions in reductive media. Although not impossible, a higher density of Mn sites is probably necessary in reductive media than in oxidative media. Alternatively, the manganese sites of MnMCM-48 catalysts may be inactive under reductive media.

3.4.2. WMnMCM-48 catalysts. After the W sites were added to the MnMCM-48 (HT) with a Si/Mn ratio of 45, *via* chemical grafting by a liquid–solid approach, the catalyst showed reasonable catalytic activity, meaning that the addition of W has a strong positive effect on the MnMCM-48 catalysts for the conversion of MCP. It must be noted that no W–Mn bonds were observed to be formed during the tungsten grafting procedure, as evidenced by the spectroscopic studies (XPS). In this situation, catalytic reaction of MCP serves as a probe to obtain information concerning possible interactions between the atoms of the two (W–Mn) components.

Prior to the catalytic tests, two treatments were applied to better understand the catalytic behavior of the tungstenomanganesosilicate mesoporous catalysts: (i) we tested the catalysts after they were dried at 100 °C and heat-treated under hydrogen for 2 h at 500 °C and (ii) after they were calcined at 500 °C and heat-treated under hydrogen for 2 h at 500 °C.

The catalytic potential of the WMnMCM-48 catalysts is presented in Fig. 8–10 as a function of the reaction temperature.

3.4.2.1. WMnMCM-48 dried at 100 °C and heat-treated under hydrogen for 2 h at 500 °C. Although the catalysts were tested between 200 and 500 °C, the W sites were inactive at temperatures less than 400 °C. These sites exhibited catalytic activity only between 400 and 500 °C. The catalytic results show a linear increase in the percent conversion in this temperature range. The values of the conversion varied between 0.69% at 400 °C and 23.40% at 500 °C (Fig. 8).

Olefins were not observed among the products over the studied temperature range (200–500 °C). No products derived from ring-opening reactions were observed, which indicates the difficulty of the endocyclic C–C bond rupture. In addition, no products derived from ring-enlargement reactions were formed. Only the C_1 products from the cracking reaction were observed as the major products. The data show that, irrespective of the temperature, the cracking-selectivity values were 100% (Fig. 8). These results reflect the fact that the WMnMCM-48 catalysts,

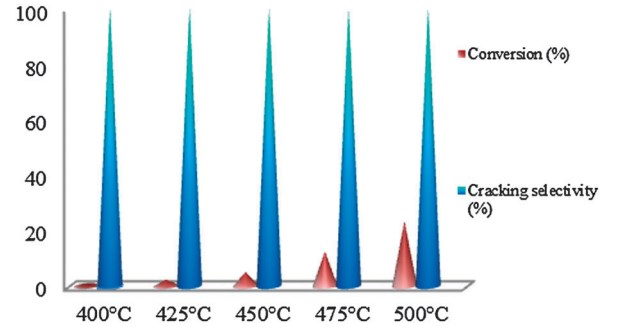

Fig. 8 Conversion of MCP on WMnMCM-48 catalysts dried at 100 °C and heat-treated under hydrogen for 2 h at 500 °C.

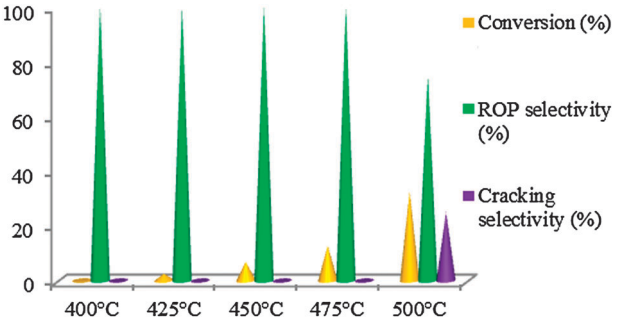

Fig. 9 Conversion of MCP on WMnMCM-48 catalysts calcined at 500 °C and heat-treated under hydrogen for 2 h at 500 °C.

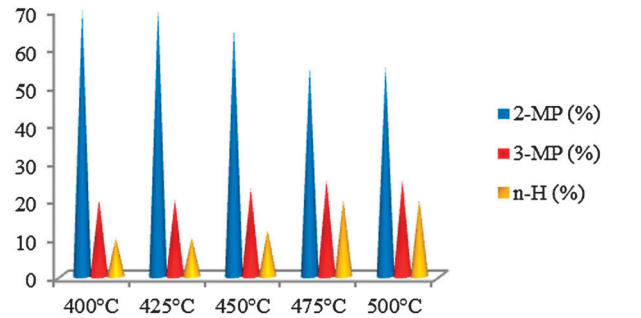

Fig. 10 Ring opening products on WMnMCM-48 catalysts calcined at 500 °C and heat-treated under hydrogen for 2 h at 500 °C.

when dried only at 100 °C, are active in extensive cracking reactions that involve successive C–C bond rupture, which underscores the poorly metallic behavior of the catalyst. It is expected that the non-calcined active sites have a low dispersion and the heat treatment under hydrogen leads to a progressive reduction of WO_3 (particles size < 5 nm) to highly reduced tungsten oxide phase W_3O with poor metallic character. In this case, on the poorly metallic sites (W_3O) the rate of desorption of the products from the WMnMCM-48 catalyst surface diminished and the multiple C–C ruptures occurred. The results may indicate strong heat adsorption of the active sites on the dried WMnMCM-48 catalyst.

Consequently, the dried WMnMCM-48 catalysts were active toward MCP conversion but not selective toward ring-opening products.

3.4.2.2. WMn-MCM-48 calcined under air at 500 °C and heat-treated under hydrogen for 2 h at 500 °C. The catalysts were tested between 200 and 500 °C, but the catalytic activity was observed starting at 400 °C (Fig. 9). At 400 and 425 °C, all the catalysts showed discrete catalytic activity, $<0.25\%$, with only traces of ring-opening products. The reactivity of the calcined WMnMCM-48 catalyst to the ring opening of MCP is slow but occurs at three positions with the formation of three products—2-MP, 3-MP and *n*-H—in different proportions (Fig. 10). This behavior is probably attributed to the high dispersion of W on the inner pore structure framework, thus resulting in a higher number of accessible active sites to MCP molecules. Under these conditions, the main role of calcinations is the redistribution of the WO_3 species over the catalyst surface and into the channels/pore of the MnMCM-48 mesoporous solid. The calcination treatments help probably to the formation of WMnMCM-48 catalysts with higher dispersion, improving in this case the accessibility of active sites. Thereafter, under hydrogen at 500 °C, as a result of dissociative chemisorption of hydrogen, the highly dispersed WO_3 species became more difficult to reduce to poorly metallic sites (W_3O) and are reduced by hydrogen atoms only to the WO_{3-x}/WO_2 phase forming Bronsted acid sites. These active acid sites are responsible for the formation of active sites for the ring opening of MCP. Furthermore, the catalytic activity gradually increased with increasing reaction temperature. Only the ring-opening products were observed at 450 and 475 °C and were considered to be the primary products under our conditions (Fig. 9). These results suggest that the formed ring opening products on highly dispersed WMnMCM-48 catalyst are strongly desorbed in the gas phase. At 500 °C, the cracking products appeared; however, the ring-opening reaction remained the major reaction. The decrease in the ring-opening selectivity at high temperatures and the high conversion are associated with cracking of the ring-opening products by the multiple ruptures of C–C bonds. As is evident from the results in Fig. 10, among the ring opening products, 2-MP is the major product. This result indicated that the catalytically active W species predominantly catalyzed the C–C rupture at unsubstituted secondary–secondary carbon atoms. The formation of only ring-opening products in the temperature range of 400 to 475 °C suggests that the catalysts possess the same active sites. The percentage of the ring-opening products, although low, decreased further with increasing temperature at 500 °C.

Taken together, the results of this study revealed that the difference in activities between the non-calcined and calcined catalysts would results not only from the W dispersion but also from the nature of W sites (W_3O or WO_{3-x}) present at the surface. Moreover, on the calcined WMnMCM-48 catalyst (WO_{3-x} sites) the ring opening products desorb easily, while on the non-calcined WMnMCM-48 catalyst (W_3O site) the ring opening products are hindered to desorb, leading to multiple ruptures of the C–C bonds.

3.4.2.3. Roles of W on catalytic activity. It must be noted that our experimental data cannot rule out the complete structure of

the WMnMCM-48 catalyst concerning the possible interaction between W and Mn and implicitly concerning the nature of active sites in the catalytic conversion of MCP. No W–Mn bonds were observed on the WMnMCM-48 catalysts, as evidenced by the spectroscopic studies (XPS). As shown in the foregoing catalytic results on MnMCM-48, the electrophilic Mn–O site was unable to catalyze the C–C bond rupture, but the introduction of W, remarkably increase the catalytic activity. Excepting the high acidity introduced by W, such change in catalytic activity could be explained by assuming that W could change the electronic properties of MnMCM-48. The special behavior of the WMnMCM-48 catalyst could be interpreted by a possible electronic interaction between W and Mn. Theoretically, the electron transfers from the low electronegative elements to high electronegative elements.[55] There is an electron transfer from the low electronegative Mn element (1.55) to the high electronegative W element (2.36). In this case, the promotion by W induces changes in the density of d electrons at the Fermi level which leads to a synergistic effect between W–Mn of the WMnMCM-48 catalyst, improving their catalytic activity. It seems that the electronic effect, which transfers electrons between Mn and W and leads to an electron-deficient state of the Mn entities, is essential for the ring opening of MCP by the rupture of secondary–secondary or secondary–tertiary bonds.

4. Conclusions

This study details our investigation of the MnMCM-48 mesoporous catalysts, prepared by three strategies, that contain Mn^{2+} and Mn^{3+} cations whose oxidation states do not change after the addition of the tungsten species, as revealed in the UV-Vis/XPS results. The introduction of Mn and W species into MCM-48-type mesoporous materials resulted in increased wall thickness, and all samples were prepared without destruction of the mesoporous cubic structure. The MnMCM-48 and WMnMCM-48 mesoporous catalysts contained either framework manganese cations or extra-framework monomolecular clusters (UV-Vis). No Mn–W bonds were observed to be formed during the tungsten grafting procedure, as evidenced by the spectroscopic studies. However, under these circumstances, the characterization is limited, which resulted in our inability to discern the electronic properties of this WMnMCM-48 mesoporous catalyst. In this situation, catalytic reaction of MCP serves as a probe to obtain information concerning possible interactions between the atoms of the two (W–Mn) components. Notably, manganese alone (electrophilic Mn–O site) was unable to catalyze the C–C bond rupture in reductive media, whereas the Mn–O sites were very active and selective in oxidative media.[24–30] Whatever the manganese content and irrespective of the reaction temperature, the MnMCM-48 did not show catalytic activity. The WMnMCM-48 catalyst did not show catalytic activity at low temperatures; however, this catalyst starts converting MCP at approximately 400 °C. The WMnMCM-48 dried at 100 °C contains active W for the successive rupture of C–C bonds by consecutive reactions but ruptures the endocyclic C–C bonds with difficulty. The WMnMCM-48 calcined at 500 °C contains active sites suitable for the endocyclic C–C bond rupture. A symbiotic process between the support and the W nanoparticles likely occurs, and a metal support effect can be envisaged in which the W particles are highly dispersed on the Mn surface of the catalysts as revealed by the catalytic tests. During the MCP conversion, W has three major functions: the acidity effect, the dispersion effect and the electronic effect. Although the conversion of MCP is relatively low, these experimental results in reductive media for WMnMCM-48 mesoporous catalysts are essential for the development and optimization of novel catalysts for the petrochemical industry.

Acknowledgements

We are pleased to acknowledge the REALISE network and the IDECAT network of excellence for their support. The generous support of the CNRS France is acknowledged with gratitude by I. Fechete.

References

1 R. J. Fenoglio, G. M. Nunez and D. E. Resasco, *Appl. Catal.*, 1990, **63**, 319.
2 P. Samoila, M. Boutzeloit, C. Especel, F. Epron and P. Marecot, *Appl. Catal., A*, 2009, **369**, 104.
3 A. Djeddi, I. Fechete and F. Garin, *Appl. Catal., A*, 2012, **413–414**, 340.
4 C. Poupin, L. Pirault-Roy, C. La Fontaine, L. Toth, M. Chamam, A. Wootsch and Z. Paal, *J. Catal.*, 2010, **272**, 315.
5 P. Samoila, M. Boutzeloit, C. Especel, F. Epron and P. Marecot, *J. Catal.*, 2010, **276**, 237.
6 A. Djeddi, I. Fechete and F. Garin, *Catal. Commun.*, 2012, **17**, 173.
7 N. Gyorffy, I. Bakos, S. Szabo, L. Toth, U. Wild, R. Schlogl and Z. Paal, *J. Catal.*, 2009, **263**, 372.
8 Z. Paal, *Catal. Today*, 1988, **2**, 595.
9 A. Djeddi, I. Fechete and F. Garin, *Top. Catal.*, 2012, **55**, 700.
10 M. Chow and G. B. McVicker, *J. Catal.*, 1988, **112**, 303.
11 G. Maire, G. Plouidy, J. C. Prudhomme and F. G. Gault, *J. Catal.*, 1965, **4**, 556.
12 M. J. Dees, M. H. B. Bol and V. Ponec, *Appl. Catal.*, 1990, **64**, 279.
13 I. Fechete, Y. Wang and J. C. Vedrine, *Catal. Today*, 2012, **189**, 2.
14 I. Fechete, B. Donnio, O. Ersen, T. Dintzer, A. Djeddi and F. Garin, *Appl. Surf. Sci.*, 2011, **257**, 2791.
15 G. Shi, D. Fang and J. Shen, *Microporous Mesoporous Mater.*, 2009, **120**, 339.
16 T. Tsoncheva, J. Rosenholm, M. Linden, F. Kleitz, M. L. Ivanova, M. Dimitrov, D. Paneva, I. Mitov and C. Minchev, *Microporous Mesoporous Mater.*, 2008, **112**, 327.
17 F. Zhang, X. Chen, J. Zhuang, Q. Xiao, Y. Zhong and W. Zhu, *Catal.: Sci. Technol.*, 2011, **1**, 1250.
18 D. Meloni, R. Monaci, E. Rombi, C. Guimon, H. Martinez, I. Fechete and E. Dumitriu, *Stud. Surf. Sci. Catal.*, 2002, **142**, 167.

19 P. C. Bakala, E. Briot, L. Salles and J.-M. Bregeault, *Appl. Catal., A*, 2006, **300**, 91.
20 E. Dumitriu, C. Guimon, V. Hulea, D. Lutic and I. Fechete, *Appl. Catal., A*, 2002, **237**, 211.
21 I. Fechete, E. Gautron, E. Dumitriu, D. Lutic, P. Caullet and H. Kessler, *Rev. Roum. Chim.*, 2008, **53**, 49.
22 E. Dumitriu, V. Hulea, I. Fechete, C. Catrinescu, A. Auroux, J. F. Lacaze and C. Guimon, *Appl. Catal., A*, 1999, **181**, 15.
23 E. Dumitriu, V. Hulea, I. Fechete, A. Auroux, J. F. Lacaze and C. Guimon, *Microporous Mesoporous Mater.*, 2001, **43**, 341.
24 S. L. Brock, N. Duan, Z. R. Tian, O. Giraldo, H. Zhou and S. L. Suib, *Chem. Mater.*, 1998, **10**, 2619.
25 Z.-R. Tang, S. A. Kondrat, C. Dickinson, J. K. Bartley, A. F. Carley, S. H. Taylor, T. E. Davies, M. Allix, M. J. Rosseinsky, J. B. Claridge, Z. Xu, S. Romani, M. J. Crudace and G. J. Hutchings, *Catal.: Sci. Technol.*, 2011, **1**, 740.
26 G. G. Xia, Y. G. Yin, W. S. Willis, J. Y. Wang and S. L. Suib, *J. Catal.*, 1999, **185**, 91.
27 S. Singha and K. M. Parida, *Catal.: Sci. Technol.*, 2011, **1**, 1496.
28 S. Gomez, L. J. Garces, J. Villegas, R. Ghosh, O. Giraldo and L. S. Suib, *J. Catal.*, 2005, **233**, 60.
29 K. M. Parida, S. S. Dash and S. Singha, *Appl. Catal., A*, 2008, **351**, 59.
30 M. Selvaraj, K. S. Seshadri, A. Pandurangan and T. G. Lee, *Microporous Mesoporous Mater.*, 2005, **79**, 261.
31 A. Boulaoued, I. Fechete, B. Donnio, M. Bernard, P. Turek and F. Garin, *Microporous Mesoporous Mater.*, 2012, **155**, 131.
32 S. Haddoum, I. Fechete, B. Donnio, F. Garin, D. Lutic and C. E. Chitour, *Catal. Commun.*, 2012, **27**, 141.
33 J. S. Beck, J. C. Vartuli, W. J. Roth, M. E. Leonowicz, C. T. Kresge, K. D. Schmitt, C. T. W. Chu, D. H. Olson, E. W. Sheppard, S. B. McCullen, J. B. Higgins and J. L. Schlenker, *J. Am. Chem. Soc.*, 1992, **114**, 10834.
34 K. Schumacher, P. I. Ravikovitch, A. Du Chesne, A. V. Neimark and K. K. Unger, *Langmuir*, 2000, **16**, 4648.
35 S. Brunauer, P. H. Emmett and E. Teller, *J. Am. Chem. Soc.*, 1938, **60**, 309.
36 E. P. Barret, L. G. Jouner and P. P. Halenda, *J. Am. Chem. Soc.*, 1951, **73**, 373.
37 M. Hartmann and C. Bischof, *J. Phys. Chem. B*, 1999, **103**, 6230.
38 K. S. W. Sing, D. H. Everett, R. A. Haul, L. Moscou, R. A. Pirroti, J. Rouquerol and T. Siemoeniewska, *Pure Appl. Chem.*, 1985, **57**, 603.
39 J. H. Scofield, *J. Electron Spectrosc. Relat. Phenom.*, 1976, **8**, 129–137.
40 S. J. Lee, A. Gavriilidis, Q. A. Pankhurst, A. Kyek, F. E. Wagner, P. C. L. Wong and K. L. Yeung, *J. Catal.*, 2001, **200**, 298.
41 S. Gomez, O. Giraldo, L. J. Garces, J. Villegas and S. L. Suib, *Chem. Mater.*, 2004, **16**, 2411.
42 P. Van Der Voort, M. Morey, G. D. Stucky, M. Mathieu and E. F. Vansant, *J. Phys. Chem. B*, 1998, **102**, 585.
43 D. Zhao and D. Goldfarb, *Stud. Surf. Sci. Catal.*, 1995, **97**, 181–188.
44 N. N. Tusar, S. Jank and R. Glaser, *ChemCatChem*, 2011, **3**, 254.
45 L. Vradman, M. V. Landau, M. Herskowitz, V. Ezersky, M. Talianker, S. Nikitenko, Y. Koltypin and A. Gedanken, *J. Catal.*, 2003, **213**, 163.
46 J. S. Foord, R. B. Jackman and G. C. Allen, *Philos. Mag.*, 1984, **49**, 657.
47 J. F. Moulder, W. F. Stickle, P. E. Sobol and K. D. Bomben, *Handbook of X-ray Photoelectron Spectroscopy*, Perkin Elmer, Eden Praitie, MN, 1992.
48 H. Cao and S. L. Suib, *J. Am. Chem. Soc.*, 1994, **116**, 5334.
49 B. J. Aronson, C. F. Blanford and A. Stein, *J. Phys. Chem. B*, 2000, **104**, 449.
50 G. Lu, X. Li, Z. Qu, Q. Zhao, H. Li, Y. Shen and G. Chen, *Chem. Eng. J.*, 2010, **159**, 241.
51 G. S. Kumar, M. Palanichamy, M. Hartmann and V. Murugesan, *Microporous Mesoporous Mater.*, 2008, **112**, 53.
52 Q. Zhang, Y. Wang, S. Itsuki, T. Shishido and K. Takehira, *J. Mol. Catal. A: Chem.*, 2002, **188**, 189.
53 C. Y. Chen, H. X. Li and M. E. Davis, *Microporous Mater.*, 1993, **2**, 17.
54 S. Velu, N. Shah, T. M. Jyothi and S. Sivasanker, *Microporous Mesoporous Mater.*, 1999, **33**, 61.
55 L. Pauling, *J. Am. Chem. Soc.*, 1932, **54**, 3570.